ISSN 1063-7788, Physics of Atomic Nuclei, 2009, Vol. 72, No. 3, pp. 410–424. © Pleiades Publishing, Ltd., 2009.
Original Russian Text © B.S. Ishkhanov, V.N. Orlin, 2009, published in Yadernaya Fizika, 2009, Vol. 72, No. 3, pp. 444–458.

NUCLEI
Theory

Description of Cross Sections for Photonuclear Reactions in the Energy Range between 7 and 140 MeV

B. S. Ishkhanov and V. N. Orlin*

Institute of Nuclear Physics, Moscow State University, Moscow, 119992 Russia

Received March 27, 2008; in final form, July 3, 2008

Abstract—A combination of the exciton and evaporation models is used to describe photonuclear reactions induced in light, medium-mass, and heavy nuclei by photons of energy in the range $7 \leq E_\gamma \leq 140$ MeV. Two mechanisms of the photoexcitation of nuclei are considered. These are the formation of a giant dipole resonance at energies in the range $E_\gamma \lesssim 30$ MeV and quasideuteron photoabsorption, which is dominant at energies in the region $E_\gamma \gtrsim 40$ MeV. The density of particle–hole states, which appears in the exciton model, is calculated on the basis of the Fermi gas model. The emission of two preequilibrium particles is taken into account in describing the quasideuteron reaction channel. The effect of isospin conservation on giant-dipole-resonance decay accompanied by photonucleon emission is examined. The model in question is used to describe cross sections for photon-induced reactions on ^{26}Mg, ^{54}Fe, ^{112,118,119,124}Sn, and ^{181}Ta nuclei.

PACS numbers: 25.20.-x
DOI: 10.1134/S1063778809030041

1. INTRODUCTION

In the energy range between 7 and 140 MeV—that is, up to the pion-production threshold—photonuclear reactions proceed predominantly via two photoabsorption mechanisms. These are the formation of a giant dipole resonance and quasideuteron photoabsorption [1]. The first prevails at energies in the range $E_\gamma \gtrsim 30$ MeV, while the second is dominant at energies in the region $E_\gamma \gtrsim 40$ MeV.

The character of photonucleon emission depends greatly on the nature of the primary excitation of a target nucleus. For example, preequilibrium nucleon emission plays a significant (dominant at high energies) role in the decay of a quasideuteron excitation (see, for instance, [2–4]), because, in quasideuteron photoabsorption, the entire hard-photon energy is transferred to a single neutron–proton pair. On the other hand, the giant-dipole-resonance component of photonuclear reactions on medium-mass and heavy nuclei is determined primarily by the evaporation of nucleons from a compound-nucleus state that arises upon the thermalization of the energy of collective dipole vibrations. The contribution of preequilibrium processes to this component plays a significant role only for light nuclei and manifests itself primarily in the region of the giant-resonance maximum, where the formation of the coherent one-particle–one-hole ($1p1h$) doorway state occurs. It should also be borne in mind that the decay properties of the giant dipole resonance in light and medium-mass nuclei ($A \lesssim 100$) are strongly affected by isospin effects, since the decay of the $T_>$ giant-dipole-resonance component is dominated by proton emission because of total-isospin conservation.

With allowance for isospin splitting, the cross section for giant-dipole-resonance formation can be calculated on the basis of the semimicroscopic model developed in [5–7]. A phenomenological expression was obtained in [8] for the quasideuteron component of the photoabsorption cross section. The parameters of this expression were estimated in [9] within the Fermi gas model.

A combination of the evaporation and preequilibrium models of photonuclear reactions is usually used to describe nucleon emission following photoabsorption. There are many different formulations of the preequilibrium approach. However, only semiclassical preequilibrium models (exciton [10–13] and hybrid [14–16] ones) and quantum-mechanical multistep preequilibrium models [17–23] are applied in practice. Quantum-mechanical models in which the probability of nucleon emission is expressed in terms of quantum-mechanical transition amplitudes describe the angular distribution of reaction products better than semiclassical models do. However, the simplicity of the application of semiclassical models and their high predictive power in describing nucleon

*E-mail: orlinvn@yandex.ru

spectra and total reaction cross sections compensate for this drawback of such models to a considerable extent, and this is the reason why they are still widely used in specific calculations [24, 25]. Very close results emerge from employing the exciton and hybrid models. It was shown in [26], however, that, in contrast to the exciton model, the hybrid model is not self-consistent. Later, the hybrid model was therefore refined by including in it a Monte Carlo simulation of the preequilibrium cascade [27, 28], but this naturally made relevant calculations much more involved.

In the present study, the exciton-model version [29] based on the Fermi gas densities of ph states is used in describing preequilibrium processes. As was shown in [29], the use of such densities makes it possible to describe satisfactorily cross sections for photonuclear reactions even in the case where one takes into account the emission of only one preequilibrium particle. This is due to the fact that the role of primary preequilibrium emission becomes more pronounced upon taking into account the energy dependence of the densities of single-particle and single-hole states in the Fermi gas model [29] and the fact that multiparticle preequilibrium emission affects more strongly the energy spectra of emitted particles than total reaction cross sections. In view of the aforesaid, we decided on restricting ourselves in calculating cross sections for photonuclear reactions to considering the emission of only primary and secondary preequilibrium particles, and this simplified the calculations considerably. The main distinction of this study from that in [29] is that we take here into account the impact of isospin effects of the giant-dipole-resonance component of photonuclear reactions; the calculations revealed that, without doing this, it is impossible to describe correctly the proton channels of the reaction in the giant-resonance region. The model being considered was applied to calculating the cross sections for the photon-induced reactions on ^{26}Mg, ^{54}Fe, ^{112,118,119,124}Sn, and ^{181}Ta nuclei.

2. DESCRIPTION OF THE MODEL

Following N. Bohr's hypothesis [30], we represent the cross section for a $(\gamma, lpkn)$ photonuclear reaction involving the emission of l protons and k neutrons in the form

$$\sigma(\gamma, lpkn; E_\gamma) = \sigma_{\rm QD}(E_\gamma) W_{\rm QD}(lpkn, E_\gamma) \qquad (1)$$
$$+ \sum_{T=T_0}^{T_0+1} \sigma_{\rm GDR}^{(T)}(E_\gamma) W_{\rm GDR}^{(T)}(lpkn, E_\gamma),$$

where E_γ is the absorbed-photon energy, $\sigma_{\rm QD}(E_\gamma)$ is the cross section for quasideuteron photoabsorption, $W_{\rm QD}(lpkn, E_\gamma)$ is the probability of quasideuteron-excitation decay involving the emission of l protons and k neutrons, $\sigma_{\rm GDR}^{(T)}(E_\gamma)$ is the isospin-T ($T_< = T_0$ or $T_> = T_0 + 1$, where T_0 is the ground-state isospin of a target nucleus) component of the cross section for giant-dipole-resonance formation, and $W_{\rm GDR}^{(T)}(lpkn, E_\gamma)$ is the probability of photonucleon emission from the corresponding giant-dipole-resonance component.

The first and the second term on right-hand side of (1) represent, respectively, the quasideuteron and giant-dipole-resonance components of the cross section for the photonucleon reaction in question: $\sigma_{QD}(\gamma, lpkn)$ and $\sigma_{\rm GDR}(\gamma, lpkn)$.

2.1. Quasideuteron Component of Photonucleon Reactions

2.1.1. Cross section $\sigma_{\rm QD}(E_\gamma)$. In the Introduction, we indicated that, in calculating this quantity, one can employ the phenomenological expression obtained in [8, 9].

2.1.2. Probability $W_{\rm QD}(lpkn, E_\gamma)$. Quasideuteron photoabsorption involves the excitation of one neutron and one proton, so that a $2p2h$ doorway state (a nucleon configuration featuring $m = m_0 = 4$ excitons) arises. This primary excitation decays either via the emission of an excited nucleon or, what is more probable, via an intranuclear transition because of the residual two-body interaction to a more complex $3p3h$ configuration, which involves $m = m_0 + 2 = 6$ excitons. After that, the system continues evolving in a similar way. The product m-exciton state either emits a nucleon into a continuum or undergoes an $m \to m + 2$ intranuclear transition, and so on. Via $m \to m + 2$ intranuclear transitions, the excitation energy of the compound system is redistributed over an ever greater number of excitons until the state of thermal equilibrium is finally attained either in the initial or in one of the residual nuclei, whereupon a comparatively long process of neutron evaporation begins (proton evaporation is suppressed by the Coulomb barrier). The reaction scheme described immediately above does not take explicitly into account inverse ($m \to m - 2$) intranuclear transitions, which do not have a strong effect on preequilibrium nucleon emission. Moreover, we indicated in the Introduction that we restrict ourselves to examining only the first two preequilibrium particles.

Under the above assumptions, the probabilities of interest can be represented in the form

$$W_{\rm QD}(lpkn, E_\gamma) \quad (2)$$
$$= \hbar \sum_{j=n,p} \sum_{\substack{m=m_0\\ \Delta m=2}}^{\bar m-2} \frac{D(m_0, m, E_\gamma)}{\Gamma^\uparrow(m, E_\gamma) + \Gamma^\downarrow(m, E_\gamma)}$$
$$\times \int_0^{E_\gamma - B_j} \lambda_j(m, \varepsilon_j, E_\gamma)$$
$$\times \Bigg[(\delta_{jn}\delta_{l0} + \delta_{jp}\delta_{l1}) I_j^{(1)}(k, m, \varepsilon_j, E_\gamma)$$
$$+ \sum_{j'=n,p} \sum_{\substack{m'=m-1\\ \Delta m'=2}}^{\bar m'-2} (\delta_{jn}\delta_{j'n}\delta_{l0}$$
$$+ \delta_{jn}\delta_{j'p}\delta_{l1} + \delta_{jp}\delta_{j'n}\delta_{l1}$$
$$+ \delta_{jp}\delta_{j'p}\delta_{l2}) I_{jj'}^{(2)}(k, m, m', \varepsilon_j, E_\gamma) \Bigg] d\varepsilon_j$$
$$+ \delta_{l0} D(m_0, \bar m, E_\gamma) P(k, E_\gamma; Z_0, N_0),$$

where $m_0 = 4$; $l + k = 1, 2, 3, \ldots$ with $l = 0, 1, 2$;

$$I_j^{(1)}(k, m, \varepsilon_j, E_\gamma) \equiv D(m-1, \bar m', U_j)$$
$$\times P(k - \delta_{jn}, U_j; Z_0 - \delta_{jp}, N_0 - \delta_{jn});$$
$$I_{jj'}^{(2)}(k, m, m', \varepsilon_j, E_\gamma) \equiv D(m-1, m', U_j)$$
$$\times \frac{\Gamma_{j'}^\uparrow(m', U_j)}{\Gamma^\uparrow(m', U_j) + \Gamma^\downarrow(m', U_j)}$$
$$\times P(k - \delta_{jn} - \delta_{j'n}, \bar U_{jj'}; Z_0 - \delta_{jp}$$
$$- \delta_{j'p}, N_0 - \delta_{jn} - \delta_{j'n});$$

$$\Gamma_j^\uparrow(n, E) = \hbar \int_0^{E - B_j} \lambda_j(n, \varepsilon_j, E) d\varepsilon_j \quad (3)$$

is the width of the n-exciton state with an excitation energy E due to the emission of a nucleon belonging to type j (a neutron, $j = n$, or a proton, $j = p$) from the initial $\{Z_0, N_0\}$ (or a residual $\{Z', N'\}$) nucleus; $\lambda_j(n, \varepsilon_j, E)d\varepsilon_j$ is the probability per unit time for the decay of such a state via the emission of a nucleon belonging to type j and having a kinetic energy $\varepsilon_j \pm d\varepsilon_j/2$ to a continuum; $\Gamma^\uparrow(n, E) = \Gamma_n^\uparrow(n, E) + \Gamma_p^\uparrow(n, E)$ is the total width of the n-exciton state with respect to nucleon emission; $\Gamma^\downarrow(n.E)$ is its spreading width caused by $n \to n + 2$ intranuclear transitions;

$$D(n, m, E) = \begin{cases} 1 \quad \text{for } m = n, \\ \displaystyle\prod_{\substack{k=n\\ \Delta k=2}}^{m-2} \frac{\Gamma^\downarrow(k, E)}{\Gamma^\uparrow(k, E) + \Gamma^\downarrow(k, E)} \\ \text{for } m = n+2, n+4, \ldots \end{cases} \quad (4)$$

is the probability that the chain of intranuclear transitions occurring in the nucleon system and starting from the n-exciton state reaches the m-exciton stage ($m = n, n+2, \ldots$); $P(k, E; Z, N)$ is the probability of the evaporation of k neutrons from the compound state of the $\{Z, N\}$ nucleus whose excitation energy is E (for $k < 0$, $P = 0$); $U_j = E_\gamma - B_j - \varepsilon_j$ is the excitation energy of the primary residual nucleus; $\bar U_{jj'} = U_j - B'_{j'} - \bar\varepsilon_{j'}(m', U_j)$ is the average excitation energy of the secondary residual nucleus formed upon the emission of a j'-type nucleon at the m'-exciton stage of the preequilibrium cascade in the primary residual nucleus; B_j and $B'_{j'}$ are the energies required for separating nucleons of types j and j' from, respectively, the target nucleus and the primary residual nucleus;

$$\bar\varepsilon_{j'}(m', U_j) = \frac{\int_0^{U_j - B'_{j'}} \lambda_{j'}(m', \varepsilon_{j'}, U_j)\varepsilon_{j'} d\varepsilon_{j'}}{\int_0^{U_j - B'_{j'}} \lambda_{j'}(m', \varepsilon_{j'}, U_j) d\varepsilon_{j'}} \quad (5)$$

is the average energy of a j'-type nucleon emitted at the m'-exciton stage of the preequilibrium cascade in the primary residual nucleus; and $\bar m = \bar m(E_\gamma)$ and $\bar m' = \bar m'(U_j)$ are the average numbers of excitons in the thermal-equilibrium states of the target nucleus and the primary residual nucleus.

By using the detailed-balance principle, Cline and Blann [10] obtained an expression for the emissive-decay rate $\lambda_j(n, \varepsilon_j, E)$ in the form

$$\lambda_j(n, \varepsilon_j, E) d\varepsilon_j = \frac{2s+1}{\pi^2\hbar^3}\mu\varepsilon_j \quad (6)$$
$$\times \sigma_j^{\rm inv}(\varepsilon_j)\frac{\omega(n-1, U_j)}{\omega(n, E)} d\varepsilon_j,$$

where s, μ, and $\sigma_j^{\rm inv}(\varepsilon_j)$ are respectively the spin, reduced mass, and inverse-reaction cross section for a j-type nucleon of energy ε_j emitted in a continuum and $\omega(n, E)$ and $\omega(n-1, U_j)$ are the densities of n- and $(n-1)$-exciton states in, respectively, the initial and the final nucleus.

The probabilities of intranuclear transitions are usually estimated in the first order of perturbation theory. This yields [21–23]

$$\Gamma^\downarrow(n, E) = 2\pi M^2(E)\omega_+(n, E), \quad (7)$$

where $M^2(E)$ is the average square of the two-body transition matrix element and $\omega_+(n, E)$ is the average density of final states accessible in the $n \to n+2$ transition.

The average square of the matrix element, $M^2(E)$, was approximated by the expression

$$M^2(E) = M^2\frac{E_{\rm res}}{E}, \quad (8)$$

where $E_{\rm res}$ is the dipole-resonance energy and the factor E^{-1} takes into account the empirical energy dependence of the square of the matrix element [11].

The constant M^2 was determined from relation (7), in which the dipole-resonance spreading width $\Gamma^{\downarrow}_{\rm res} \equiv \Gamma^{\downarrow}(2, E_{\rm res})$ was estimated on the basis of expression (9) (see below). The densities of states $\omega(n, E)$, $\omega(n-1, U)$, and $\omega_{+}(n, E)$, which appear in expressions (6) and (7), can be calculated on the basis of the Fermi gas model. On one hand, this choice of density of states correlates with the method proposed by Chadwick et al. [9] for estimating the parameters of the quasideuteron photoabsorption model; on the other hand, it permits taking into account the effect of the energy dependence of the density of single-particle and single-hole states (in particular, the vanishing of the density of single-hole states at energies in excess of the Fermi energy, $\varepsilon_{\rm F} \approx 35$ MeV) on the dynamics of the development of the preequilibrium cascade. A procedure for calculating Fermi gas densities of particle–hole states is described in [29].[1)] A method for calculating the probability of multiparticle neutron evaporation, $P(k, E; Z, N)$, from the compound-nucleus state was also proposed there.

2.2. Giant-Dipole-Resonance Component of Photonuclear Reactions

2.2.1. Cross sections $\sigma^{(T)}_{\rm GDR}(E_\gamma)$, $T = T_<, T_>$. According to the aforesaid (see Introduction), the $T_<$ and $T_>$ components of the giant dipole resonance can be calculated within the semimicroscopic model proposed in [5–7]. The spreading width of an individual dipole resonance can be estimated by means of the semiempirical formula [7]

$$\Gamma^{\downarrow}_{\rm res} \approx GI(a_0/R_0)[E_{\rm res} - \Delta(Z_0, N_0)\delta_{TT_>}]^2, \quad (9)$$

where

$$I(\xi) = \left[1 - 3\xi(1 + \pi^2\xi^2/3)/(1 + \pi^2\xi^2)\right]/(1 + \pi^2\xi^2)$$

is a dimensionless factor that determines the dependence of the spreading width on the diffuseness of the nuclear surface [31]; a_0 and R_0 are parameters that characterize, respectively, the diffuseness and the radius of the Fermi distribution of the nucleon density; $E_{\rm res}$ is the resonance energy; Δ is the energy of the first excited state of the nucleus being considered for the isospin of $T = T_>$ [this energy is introduced in (9) in order to take into account the shift upward of accessible $2p2h$ states to which the $T_>$ resonance decays]; and G is a normalization constant.

In the present study, the parameter R_0 was set to $1.07A^{1/3}$ fm (in accordance with electron-scattering data). The energy Δ was estimated on the basis of the change in the Coulomb energy and the binding energy of the nucleon system upon going over from the $\{Z_0, N_0\}$ to the $\{Z_0 - 1, N_0 + 1\}$ nucleus. The remaining parameters a_0 and G were fitted to experimental values of the dipole-resonance widths for a large number of nuclei (with allowance for the width with respect to nucleon emission—see below). This eventually yielded the values of $a_0 = 0.685$ fm and $G = 0.0328\ \mathrm{MeV}^{-1}$.

The dipole-resonance width with respect to nucleon emission, $\Gamma^{\uparrow}_{\rm res}$, can be calculated by formulas (3) and (6) at $n = 2$, the substitution $B_n \to B_n + \Delta(Z', N')\delta_{TT_>}$ being necessary for the neutron channel of of $T_>$-resonance decay. This substitution makes it possible to take into account the decrease in the $T_>$-resonance width with respect to nucleon emission because of the shift upward of $(n-1)$-exciton states whose isospin is $T'_> = T'_0 + 1$ (where T'_0 is the ground-state isospin of the $\{Z', N'\}$ residual nucleus). We note that it is unnecessary to introduce any other changes in expressions (3) and (6), since, for the $T_>$ reaction channel, the densities of states $\omega(n, E)$ and the cross section $\sigma^{inv}_n(\varepsilon_n)$ decrease to the same degree in relation to their total values.

2.2.2. Probabilities $W^{(T)}_{\rm GDR}(lpkn, E_\gamma)$. The preequilibrium decay of giant dipole resonances can proceed via nucleon emission from a $1p1h$ collective doorway state. This state is formed in the region of the dipole-resonance maximum. Above (and below) the maximum of the T giant-dipole-resonance component, the contribution of the primary collective excitation to the dipole-state wave function decreases in proportion to the ratio $q^{(T)}(E_\gamma) = \sigma^{(T)}_{\rm GDR}(E_\gamma)/\max(\sigma^{(T)}_{\rm GDR}(E_\gamma))$. Taking this circumstance into account, we represent the probability of the emission of l protons and k neutrons from the T giant-dipole-resonance component in the form

$$W^{(T)}_{\rm GDR}(lpkn, E_\gamma) = \hbar q^{(T)}(E_\gamma) \quad (10)$$
$$\times \sum_{j=n,p} \sum_{\substack{m=m_0 \\ \Delta m=2}}^{\bar{m}-2} \frac{D^{(T)}(m_0, m, E_\gamma)}{\Gamma^{(T)\uparrow}(m, E_\gamma) + \Gamma^{(T)\downarrow}(m, E_\gamma)}$$

[1)]In [29], a factor of 1/2 is missing in expression (25), which determines (with allowance for the two-component composition of the nucleon system) the normalization constant for the density states $\omega(n-1, U)$.

$$\times \int_0^{E_\gamma - B_j - \Delta(Z',N')\delta_{jn}\delta_{TT_>}} \lambda_j^{(T)}(m, \varepsilon_j, E_\gamma)$$
$$\times S^{(T')}(l - \delta_{jp}, k - \delta_{jn}, U_j; Z', N') d\varepsilon_j$$
$$+ \left(1 - q^{(T)}(E_\gamma) + q^{(T)}(E_\gamma) D^{(T)}(m_0, \bar{m}, E_\gamma)\right)$$
$$\times S^{(T)}(l, k, E_\gamma; Z_0, N_0),$$

where $m_0 = 2$; $T' = T'_0 + \delta_{jn}\delta_{TT_>}$ (T'_0 is the ground-state isospin of the $\{Z' = Z_0 - \delta_{jp}, N' = N_0 - \delta_{jn}\}$ residual nucleus formed upon the emission of a j-type nucleon from a target nucleus); and $S^{(T)}(l, k, E; Z, N)$ is the probability for the evaporation of l protons and k neutrons from the compound state of the initial or the residual nucleus having an isospin $T = T_<$, $T_>$ and an excitation energy E ($S = 0$ at l or k smaller than 0).

In calculating the quantities $\lambda_j^{(T)}(m, \varepsilon_j, E)$, $\Gamma^{(T)\uparrow}(m, E)$, $\Gamma^{(T)\downarrow}(m, E)$, and $D^{(T)}(m_0, m, E)$ (with allowance for isospin conservation), not only do we introduce corrections mentioned at the end of Subsection 2.2.1, but it is also necessary to make the substitution $\omega_+(n, E) \to \omega_+(n, E - \Delta(N_0, Z_0)\delta_{TT_>})$ in Eq. (7).

The probabilities $S^{(T)}(l, k, E; Z, N)$ satisfy the recursion relation

$$S^{(T)}(l, k, E; Z, N) = \left[\int_0^{E - B_p} \varepsilon_p \sigma_p^{\text{inv}}(\varepsilon_p) \right. \quad (11)$$
$$\times w(U_p) S^{(T'_0)}(l - 1, k, U_p; Z', N) d\varepsilon_p$$
$$+ \int_0^{E - B_n - \Delta(Z,N')\delta_{TT_>}} \varepsilon_n \sigma_n^{\text{inv}}(\varepsilon_n)$$
$$\times w(U_n - \Delta(Z, N')\delta_{TT_>})$$
$$\left. \times S^{(T')}(l, k - 1, U_n; Z, N') d\varepsilon_n \right]$$
$$\times \left[\int_0^{E - B_p} \varepsilon_p \sigma_p^{\text{inv}}(\varepsilon_p) w(U_p) d\varepsilon_p \right.$$
$$+ \int_0^{E - B_n - \Delta(Z,N')\delta_{TT_>}} \varepsilon_n \sigma_n^{\text{inv}}(\varepsilon_n)$$
$$\left. \times w(U_n - \Delta(Z, N')\delta_{TT_>}) d\varepsilon_n \right]^{-1},$$

where $T' = T'_0 + \delta_{TT_>}$; $U_j = E - B_j - \varepsilon_j$ ($j = p, n$); $Z' = Z - 1$; $N' = N - 1$; and

$$w(E) \propto (E + 1/a)^{-2} \exp(2\sqrt{aE}) \qquad (12)$$

is the nuclear-level density, with a being the level-density parameter. In the following, we assume that

$$S^{(T'_0)}(l, k, E; Z', N') = \delta_{l0} P(k, E; Z', N')$$
$$\text{for } Z' + N' \le Z_0 + N_0 - 1,$$

$$S^{(T'_0+1)}(l, k, E; Z', N') = \delta_{l0} P(k, E; Z', N')$$
$$\text{for } Z' + N' \le Z_0 + N_0 - 2.$$

This means that we disregard the emission of protons in the $T_<$ and $T_>$ reaction channels, starting from, respectively, the primary and the secondary residual nucleus. This assumption seems quite reasonable since the bulk of protons are emitted in the region of the maximum of the $T_>$ giant-dipole-resonance component at relatively low excitation energies of the nucleus. At the same time, it permits employing the recursion relation (11) to calculate the nucleon-emission probabilities appearing in (10). In turn, this makes it possible to calculate the probabilities $W_{\text{GDR}}^{(T)}(lpkn, E_\gamma)$ at $l + k = 1, 2, 3, \ldots$ and $l = 0, 1$.

3. APPLICATION OF THE MODEL TO DESCRIBING THE CROSS SECTIONS FOR THE PHOTONUCLEAR REACTIONS ON Mg, Fe, Sn, AND Ta NUCLEI

3.1. Details of the Computational Procedure Used

The quadrupole-deformation parameter β of the nucleus being considered is the only free parameter of the semimicroscopic model developed in [5–7]. It was estimated by using data on the static quadrupole moments of this nucleus [32]. The inverse-reaction cross sections $\sigma_p^{inv}(\varepsilon)$ and $\sigma_n^{inv}(\varepsilon)$ [see Eqs. (6) and (11)] were calculated on the basis of the approximate expressions quoted in the monograph of Barashenkov and Toneev [33].

The level-density parameter a, the average number $\bar{m}$ of excitons in the thermal-equilibrium state, and the constant M^2 determining the rate of intranuclear transitions are the intrinsic parameters of the model being considered. Methods for estimating M^2 were discussed above (see Subsection 2.1.2). The remaining two parameters were estimated in just the same way as in [29].

The calculations involved evaluating the cross sections for the $(\gamma, lpkn)$ reactions, $l = 0, 1, 2$ and $k \le 12$, on ^{26}Mg, ^{54}Fe, ^{112,118,119,124}Sn, and ^{181}Ta nuclei in the energy range $7 \le E_\gamma \le 140$ MeV with a step of 0.1 MeV. In addition, the spectrum of

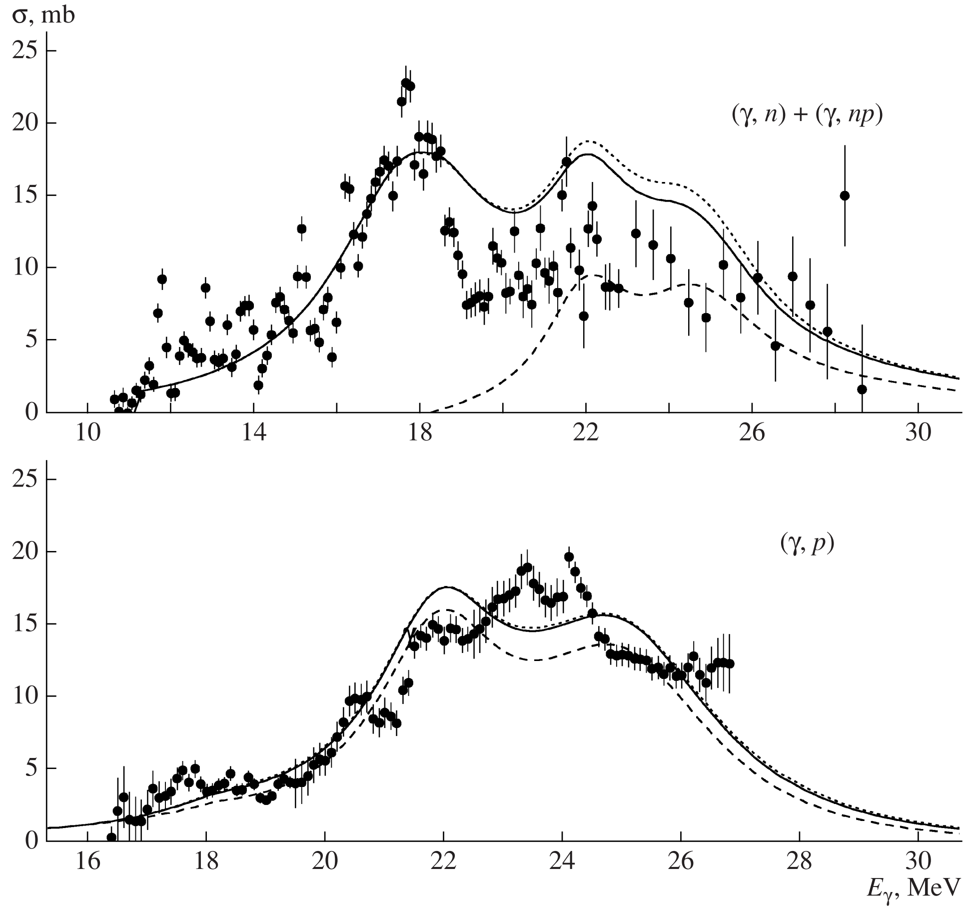

Fig. 1. Comparison of the calculated and experimental photonuclear cross sections for the $(\gamma,n)+(\gamma,np)$ and (γ,p) reactions on the ^{26}Mg nucleus in the region of the giant-dipole-resonance maximum: (points with error bars) experimental data from [34, 35], (solid curves) calculated total cross sections, (dashed curves) contribution to these cross sections from the $T_>$ giant-dipole-resonance component, and (dotted curves) results calculated for the total cross sections upon the substitution $M^2 \to M^2/2$.

primary protons was calculated for the ^{26}Mg nucleus, and the result was then transformed into partial cross sections for several groups of levels of the final nucleus ^{25}Na.

3.2. Discussion of the Results

The basic results of our calculations are presented in Figs. 1–8. These data make it possible to assess the degree of applicability of the model to light, medium-mass, and heavy nuclei and to study the contributions of various photodisintegration mechanisms, as well as to analyze the impact of isospin effects on the relative yield of protons and neutrons in the region of the giant-dipole-resonance maximum.

In Fig. 1, the experimental cross sections from [34, 35] (points with error bars) for the $(\gamma,n)+(\gamma,np)$ and (γ,p) reactions on the ^{26}Mg nucleus are contrasted against their calculated counterparts (solid curves). The dashed curves represent the contribution of the $T_>$ giant-dipole-resonance component to the theoretical cross sections. This figure shows that, in the region of $T_>$ resonances ($E_\gamma \gtrsim 20$ MeV), this component exhausts a significant part of the cross-section sum $\sigma(\gamma,n)+\sigma(\gamma,np)$ and makes a dominant contribution to the (γ,p) cross section. The theoretical curves fail to describe the intermediate structure of the experimental cross sections, since the calculation of the photoabsorption cross sections $\sigma^{(T)}_{\rm GDR}(E_\gamma)$ relied on the semimicroscopic model that was developed in [5–7] and in which the effect of single-particle dipole transitions on the structure of giant dipole resonances was disregarded. At the same time, the calculation reproduces fairly well the global features of the cross sections being considered (in particular, the relative yield of protons and neutrons).

For ^{26}Mg or other light nuclei, there is unfortunately no experimental data on cross sections for $(\gamma,lpkn)$ $(l+k=1,2,3,\ldots)$ photonuclear reactions

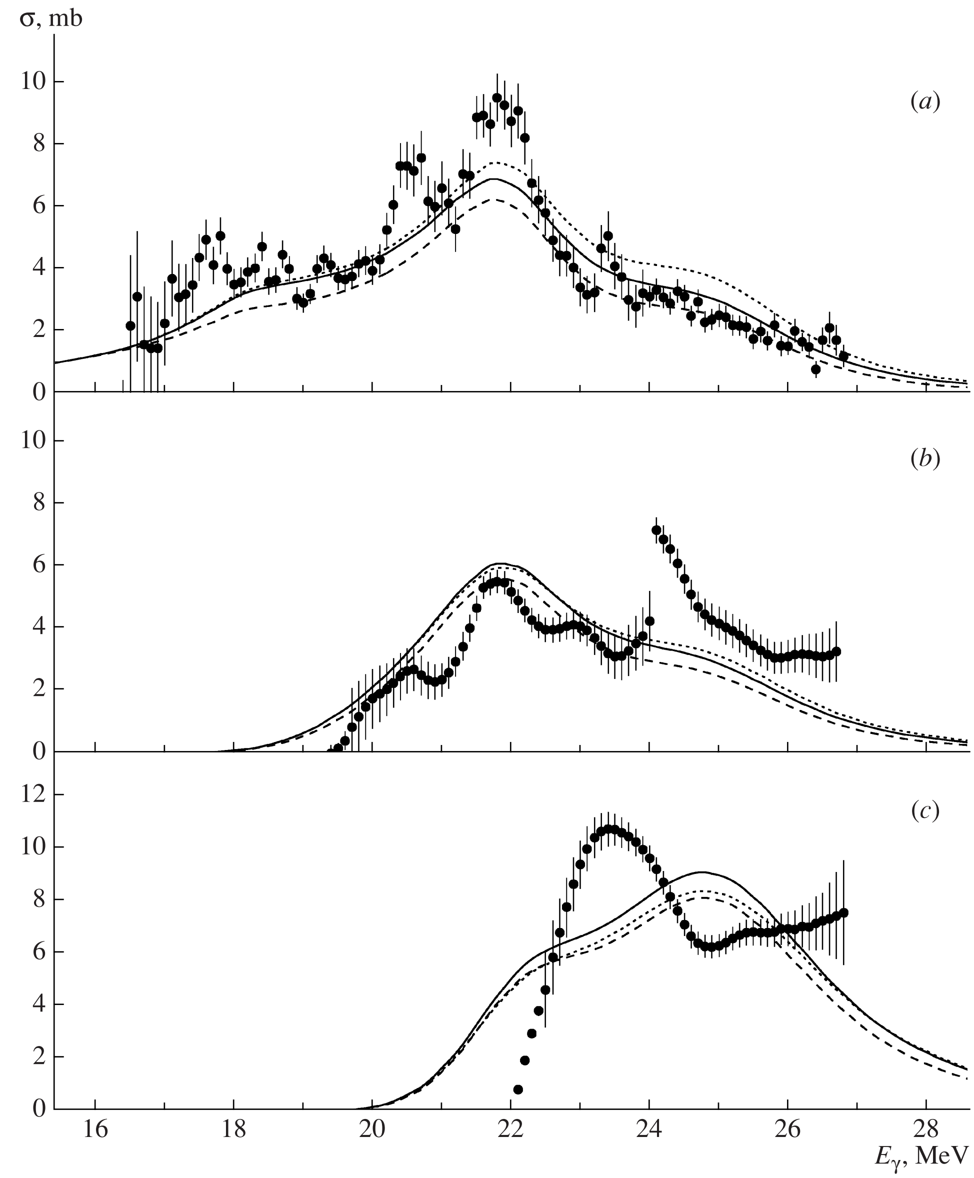

Fig. 2. Partial cross sections for photoproton reactions on the ^{26}Mg nucleus that correspond to the population of individual groups of states of the final nucleus: (a) results for the population of the ground state and the first excited state, (b) results for the population of a group of levels characterized by an average energy of 3 MeV, and (c) results for the population of a group of levels characterized by an average energy of 4 MeV. The points with error bars represent experimental data from [35]. The notation for the curves is identical to that for Fig. 1.

at high energies E_γ, and this is an obstacle to investigating the possibility of applying the model in question (without further refining its parameters) to light nuclei in the energy region above the giant dipole resonance. In particular, it is not certain that the estimate of the parameter M^2 on the basis of an analysis of experimental giant dipole-resonance widths (see Subsections 2.1.2 and 2.2.1) is correct for light nuclei, in which case $\Gamma^{\uparrow}_{\text{res}} \sim \Gamma^{\downarrow}_{\text{res}}$.

The calculations revealed that the cross sections for photonuclear reactions on light nuclei in the giant-dipole-resonance region are only slightly sensitive to the choice of value for the parameter M^2. Indeed, a decrease in this parameter by a factor of two in relation to the estimate following from relations (7)–(9) leads to only an insignificant change in the cross sections calculated for the $(\gamma, n) + (\gamma, np)$ and (γ, p) reactions on the ^{26}Mg nucleus (compare the solid and dotted curves in Fig. 1).

In [35], the partial cross sections for the photoproton reactions occurring on the ^{26}Mg nucleus and involving the excitation of individual groups of levels

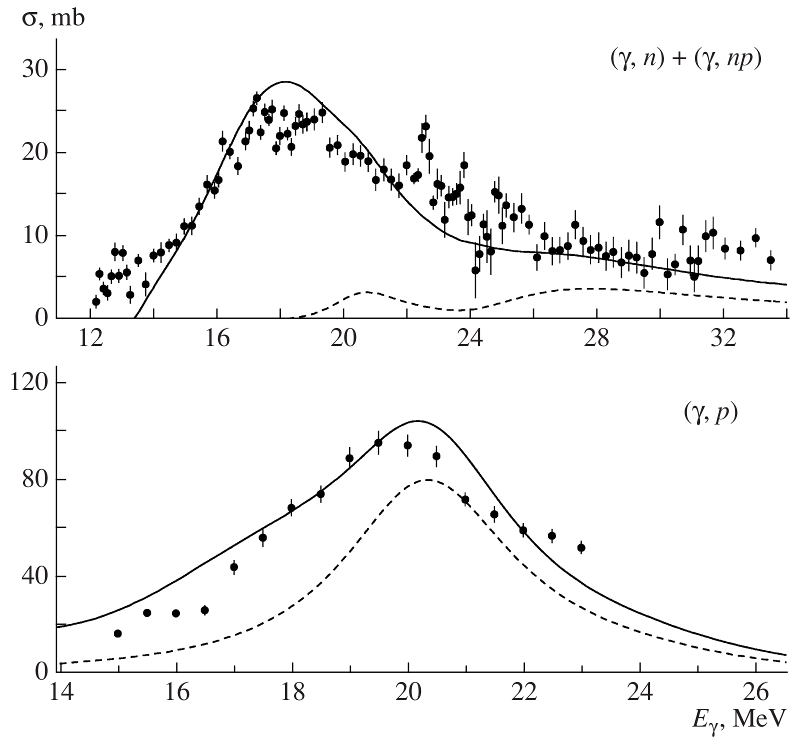

Fig. 3. Calculated and experimental photonuclear cross sections for the $(\gamma, n) + (\gamma, np)$ and (γ, p) reactions on the ^{54}Fe nucleus in the region of the giant-dipole-resonance maximum. The points with error bars represent experimental data from [36, 37]. The notation for the curves is identical to that for Fig. 1.

of the final nucleus ^{25}Na (specifically, the ground state of this nucleus and its first excited state, as well as groups of levels whose average energies are 3 and 6 MeV) were estimated on the basis of an analysis of proton spectra in the reactions induced by bremsstrahlung photons. The exciton model, which deals with continuous level densities, disregards shell effects. Therefore, it is able to describe real nuclear-level densities only at rather high excitation energies, in which case nuclear levels are condensed. The ground state of the ^{25}Na nucleus and its first excited state are separated from the other states of this nucleus by an energy gap of about 2 MeV. Taking this circumstance into account, we determined the partial cross sections of interest by integrating the spectra of primary protons from ^{26}Mg with respect to the energy $U = E_\gamma - B_p - \varepsilon_p$ of the final nucleus over the intervals [0, 2], [2, 4] and [4, 8] MeV. The results of these calculations are given in Fig. 2 (solid curves), where they are contrasted against experimental data from [35] (points with error bars). The dashed curves represent the contribution of the $T_>$ giant-dipole-resonance component to the theoretical cross sections, while the dotted curves correspond to the calculation of partial cross sections with the parameter M^2 reduced by a factor of two. This figure shows that, in just the same way as in case of the total cross sections, the results of the calculations depend only slightly on the choice of value for the parameter M^2.

In Fig. 3, the calculated cross sections for the $(\gamma, n) + (\gamma, np)$ and (γ, p) reactions on the ^{54}Fe nucleus are contrasted against their experimental counterparts from [36, 37]. In relation to ^{26}Mg, a considerable increase in the yield of protons with respect to the yield neutrons is observed here (compare Figs. 3 and 1), which is explained by a relatively low proton threshold in ^{54}Fe ($B_p - B_n = -4.5$ MeV versus $B_p - B_n = +3$ MeV in ^{26}Mg).

Having performed a separation of neutron yields in multiplicity, a group from Saclay measured the cross sections $\sigma_j(E_\gamma)$, $2 \le j \lesssim 10$, for reactions involving the emission of j or more neutrons and any number of charged particles into a continuum and occurring on nuclear targets from natural mixtures of some isotopes at energies in the range 25–132 MeV [38]. In the model being considered, such cross sections can be expressed in terms of the $(\gamma, lpkn)$ cross sections introduced in Section 2 [see formula (1)] as

$$\sigma_j(E_\gamma) = \sum_{l=0}^{2} \sum_{k=j}^{\infty} \sigma(\gamma, lpkn; E_\gamma). \tag{13}$$

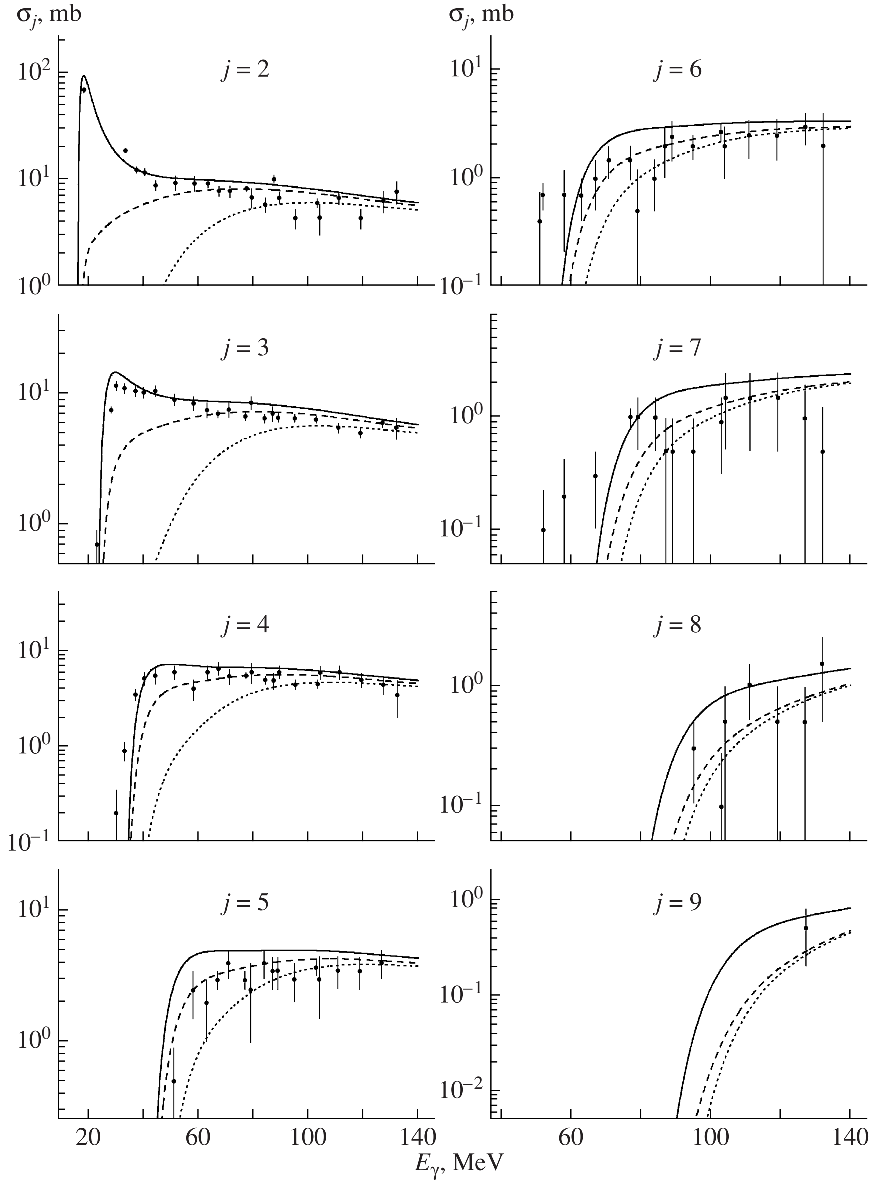

Fig. 4. Cross sections $\sigma_j(E_\gamma)$ for the photonuclear reactions occurring on tin nuclei and involving the emission of $j, j+1, \ldots$ neutrons and an arbitrary number of charged particles: (points with error bars) experimental data for a target from natural tin [38], (solid curves) cross sections calculated for the ^{119}Sn nucleus, (dashed curves) quasideuteron components of the theoretical cross sections, and (dotted curves) contribution of secondary preequilibrium processes to the quasideuteron component.

Figure 4 displays the theoretical cross sections $\sigma_j(E_\gamma)$ (solid curves) calculated for the ^{119}Sn nucleus whose mass number is the closest to the average mass number of a natural target from tin. They are compared with experimental data (points with error bars) obtained in [38]. The dashed curves represent the total quasideuteron component of the theoretical cross sections. The dotted curves stand for the contribution to this component from processes involving the emission of two preequilibrium particles. From this figure, one can see that the results of the calculations are in fairly good agreement with experimental data. A systematic excess of the calculated cross sections above the respective experimental values in the energy range $60 \lesssim E_\gamma \lesssim 120$ MeV may be due to the fact that, in this energy range, the theoretical photoabsorption curve goes markedly above the experimental data from [38], primarily because of the quasideuteron component (see [29]) calculated within the model proposed in [8, 9]. The inclusion of secondary preequilibrium emission made it possible to improve somewhat agreement with the experimental

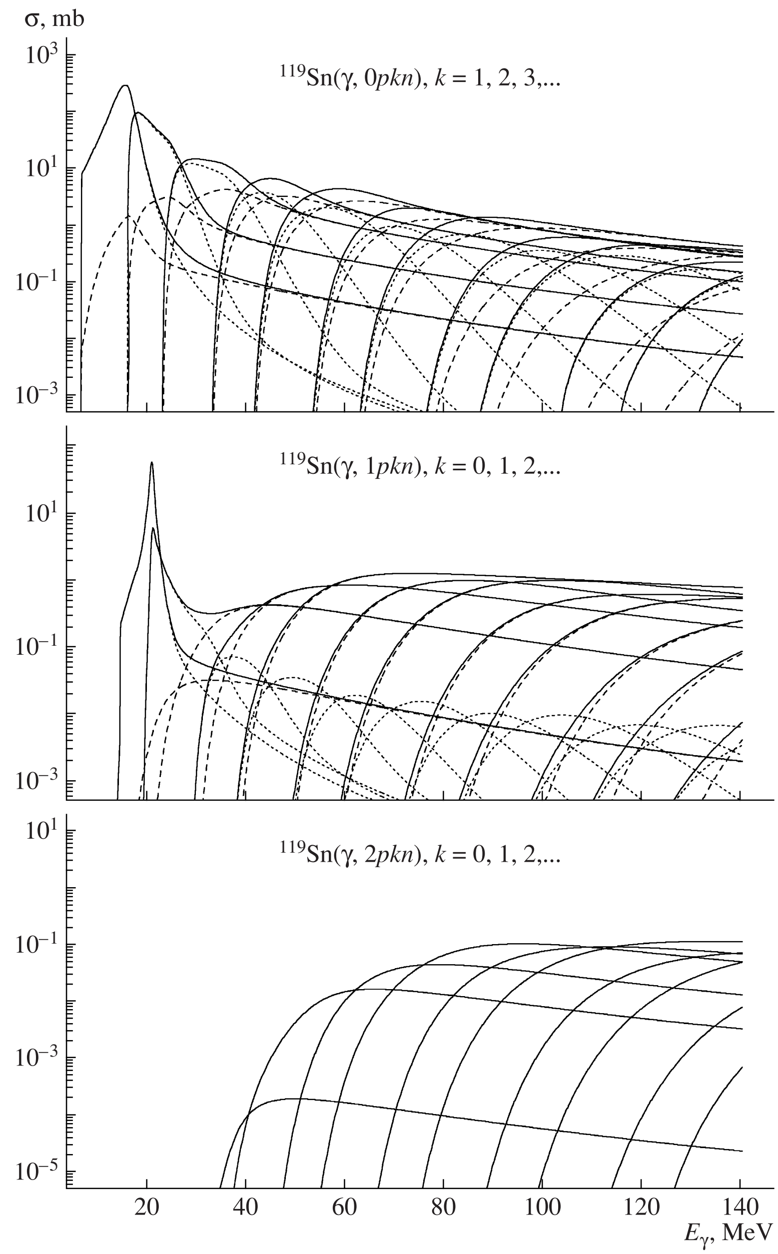

Fig. 5. Calculated photonuclear cross sections for the $(\gamma, lpkn)$ reactions on the ^{119}Sn nucleus: (solid curves) total reaction cross sections and (dashed and dotted curves) quasideuteron and giant-dipole-resonance components of these cross sections, respectively.

data in relation to the calculation reported in [29], where we took into account only primary preequilibrium processes, and, what is more important, revealed that, at high excitation energies, a dominant contribution to the quasideuteron reaction component comes from processes accompanied by the emission of more than one prequilibrium particle (compare the behavior of the dashed and dotted curves in Fig. 6). In addition, one can see a shift of quasideuteron nucleon emission toward a smaller number of emitted particles, with the result that the role of giant-dipole-resonance emission becomes more pronounced for $\sigma_j(E_\gamma)$ corresponding to large values of j.

The total set of cross sections calculated for the ^{119}Sn nucleus is displayed in Fig. 5. In the two upper panels, the cross sections calculated for the $(\gamma, lpkn)$ $(l + k = 1, 2, 3, \ldots; l = 0, 1)$ reactions (solid curves) are given along with their quasideuteron and giant-dipole-resonance components (dashed and dotted curves, respectively) in the energy range $7 \leq E_\gamma \leq 140$ MeV. From an analysis of these data, one can conclude that the giant-dipole-resonance reaction

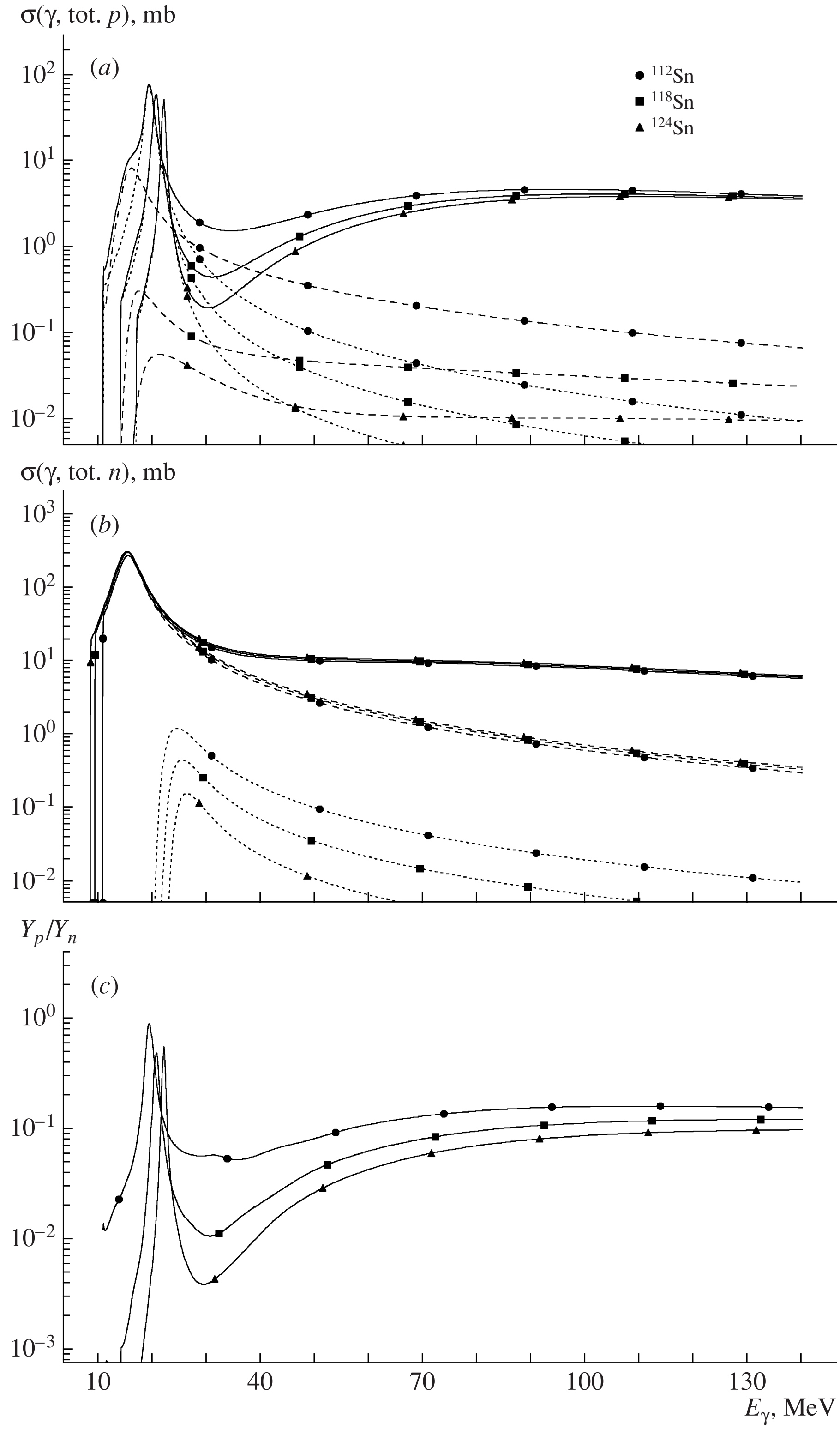

Fig. 6. Effect of the change in the isospin of the nucleus being considered on proton and neutron emission from the tin isotopes ^{112,118,124}Sn. In Figs. 6*a* and 6*b*, the solid curves represent photoproton and photoneutron cross sections, while the dashed and dotted curves stand for, respectively, the $T_<$ and the $T_>$ giant-dipole-resonance component of these cross sections. Figure 6*c* shows the ratio of the total proton and neutron yields.

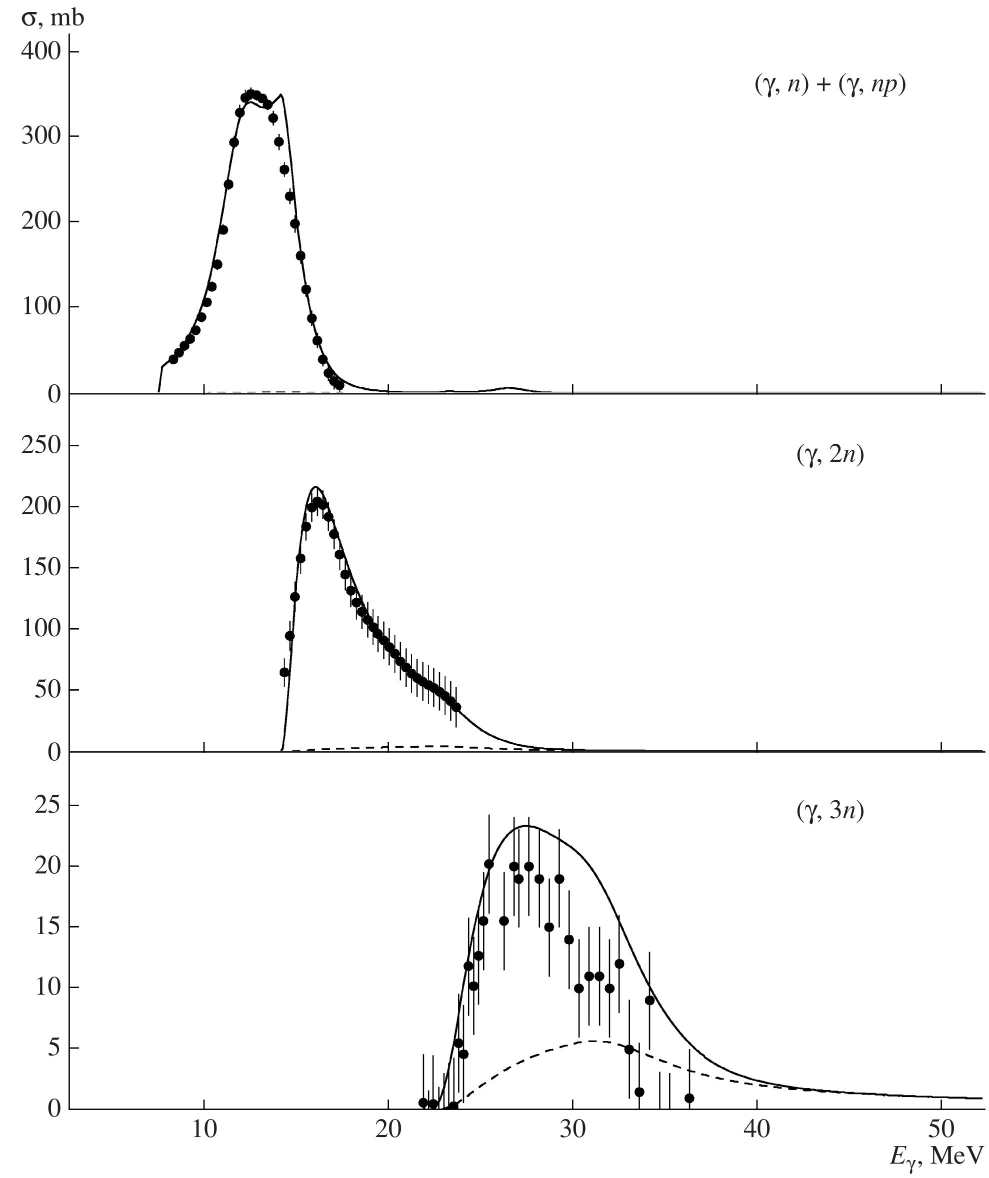

Fig. 7. Calculated and experimental photoneutron cross sections for the $(\gamma, n) + (\gamma, np)$, $(\gamma, 2n)$, and $(\gamma, 3n)$ reactions on the ^{181}Ta nucleus. The points with error bars represent experimental data from [41]. The solid and dashed curves stand for, respectively, the calculated cross sections and their quasideuteron components.

component plays a dominant role both in the neutron and in the proton channel of tin disintegration near the reaction threshold and at low excitation excitation energies of the nucleus ($E_\gamma \lesssim 40$ MeV), but that it then decreases fast with increasing energy, especially in the proton channel. The lowest panel in Fig. 5 shows the calculated cross sections for $(\gamma, 2pkn)$ reactions. It should be noted that, within the model considered here, the emission of more than one proton is considered only in the quasideuteron reaction channel (see the discussion of the quasideuteron and giant-dipole-resonance reaction components in Subsections 2.1 and 2.2).

For tin isotopes, we studied the effect of the change in the isospin of the nucleus, $T_0 = (N - Z)/2$, on proton and neutron photoemission. For this purpose, we calculated the total photoproton and photoneutron cross sections for ^{112,118,124}Sn nuclei,

$$\sigma(\gamma, \text{tot. } p) = \sum_{l=1}^{2} \sum_{k=0}^{\infty} \sigma(\gamma, lpkn; E_\gamma), \tag{14}$$

$$\sigma(\gamma, \text{tot. } n) = \sum_{l=0}^{2} \sum_{k=1}^{\infty} \sigma(\gamma, lpkn; E_\gamma), \tag{15}$$

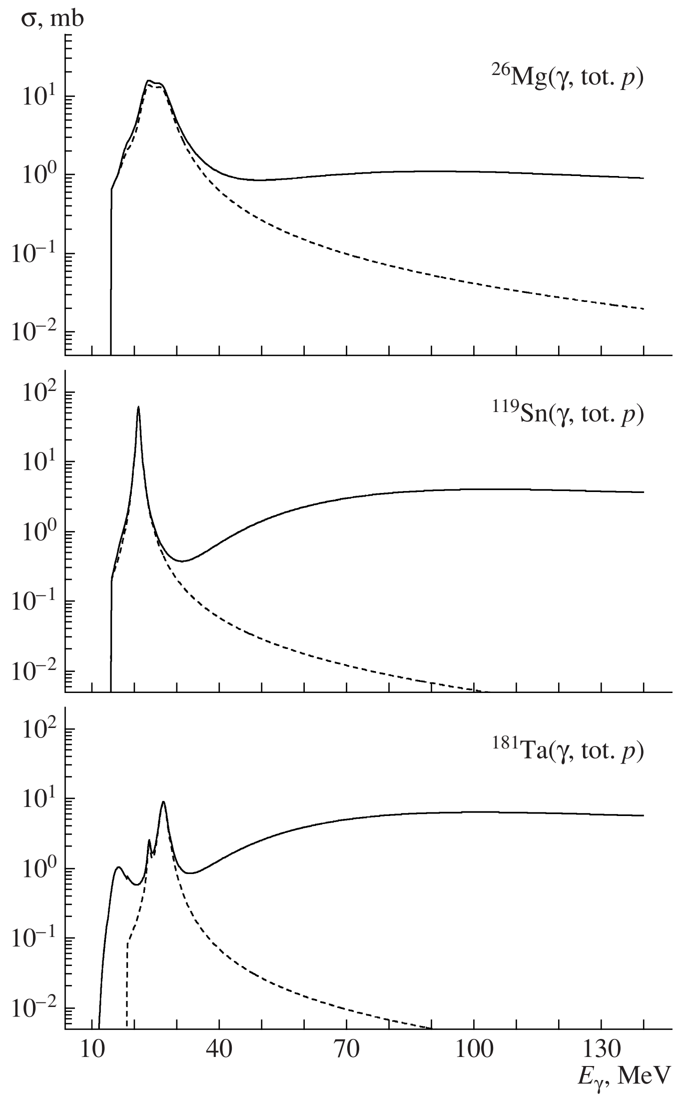

Fig. 8. Effect of the $T_>$ component of the giant dipole resonance on photoproton emission from ^{26}Mg, ^{119}Sn, and ^{181}Ta nuclei. The solid and dashed curves represent, respectively, the total photoproton cross sections and their $T_>$ giant-dipole-resonance components.

and the ratio of the total yield of protons to the total yield of neutrons,

$$Y_p/Y_n = \sum_{l=1}^{2}\sum_{k=0}^{\infty} l\sigma(\gamma, lpkn; E_\gamma) \Big/ \sum_{l=0}^{2}\sum_{k=1}^{\infty} k\sigma(\gamma, lpkn; E_\gamma). \quad (16)$$

These data are displayed in Fig. 6. In Figs. 6*a* and 6*b*, the cross sections for the reactions $^{112,118,124}\mathrm{Sn}(\gamma, \mathrm{tot.}\ p)$ and $^{112,118,124}\mathrm{Sn}(\gamma, \mathrm{tot.}\ n)$ (solid curves) are given along with their $T_<$ and $T_>$ giant-dipole-resonance components (dashed and dotted curves, respectively). Figure 6*a* shows that photoproton emission from the $T_>$ giant-dipole-resonance component is dominant in the region of low energies ($E_\gamma \lesssim 30$ MeV). Therefore, the maximum of the photoproton peak undergoes a shift toward higher energies, while its area decreases with increasing isospin of the nucleus, as is predicted in the theory of the isospin splitting of giant resonances [39, 40]. A gradual decrease in the width of these peaks as one moves along the $^{112}\mathrm{Sn} \to {}^{124}\mathrm{Sn}$ chain is also worthy of note. This is due to a simultaneous increase in $\Delta(Z_0, N_0)$ [see Eq. (9)]. At the same time (see Fig. 6*b*), the photoneutron cross sections for different tin isotopes differ only slightly from one another, since, in the giant-resonance region, they are determined by processes involving the decay of the $T_<$ giant-dipole-resonance component. From Figs. 6*a* and 6*b*, it also follows that, at high excitation energies of the nucleus ($E_\gamma > 40$ MeV), proton and neutron emission is due primarily to quasideuteron photodisintegration.

Figure 6*c* illustrates the ratio of the proton and neutron yields for various tin isotopes. This figure shows that, in a comparatively narrow energy region around the maximum of the $T_>$ giant-dipole-resonance component, one can expect commensurate yields of protons and neutrons, even though proton emission is strongly suppressed by the Coulomb barrier. This commensurability is due exclusively to the impact of isospin effects.

Among the nuclei considered here, that of ^{181}Ta was the heaviest. In Fig. 7, the calculated cross sections for the $(\gamma, n) + (\gamma, np)$, $(\gamma, 2n)$, and $(\gamma, 3n)$ reactions on the ^{181}Ta nucleus in the energy region $E_\gamma \gtrsim 40$ MeV (solid curves) are contrasted against their experimental counterparts (points with error bars) [41]. The dashed curves represent the quasideuteron-component contribution to the theoretical cross sections. Figure 7 shows that the cross sections being considered are determined primarily by processes caused by giant-dipole-resonance decay. Quasideuteron photoabsorption plays a significant role only in the formation of the cross section $\sigma(\gamma, 3n)$.

In the high-energy region ($E_\gamma > 40$ MeV), basic features of the behavior of the neutron and proton cross sections for the ^{181}Ta and ^{119}Sn nuclei are approximately identical (see Figs. 4 and 5). However, the proton yield is seen to decrease substantially with increasing mass number A.

Our investigations have revealed that isospin effects have a crucial impact on the formation of photoproton cross sections in the region of the giant-dipole-resonance maximum both in light and in heavy nuclei. This is demonstrated by Fig. 8, where the total photoproton cross sections for ^{26}Mg, ^{119}Sn, and ^{181}Ta nuclei (solid curves) are given along with their components (dashed curves) caused by the decay of isospin-$T_>$ dipole resonances.

4. CONCLUSIONS

Our calculations have demonstrated that the model considered here makes it possible to obtain a satisfactory description of cross sections for photonucleon reactions occurring on medium-mass and heavy nuclei in the energy range between 7 and 140 MeV.

For the light nucleus ^{26}Mg, we have obtained qualitative agreement between the theoretical and experimental data in the giant-dipole-resonance region. However, the question of whether the model in question (at the above choice of parameter values) is applicable at high excitation energies of nuclei has remained open. In order to test the model further, it is necessary to measure cross sections for $(\gamma, lpkn)$, $k + l = 1, 2, 3, \ldots$, photonucleon reactions on light nuclei in the region above the giant resonance.

A strong impact of isospin effects on photoproton emission in the region of the giant-dipole-resonance maximum has been demonstrated for all nuclei considered here. Among other things, it has been found that not only for light but also for medium-mass nuclei may the proton yield in the region of the giant-dipole-resonance maximum be commensurate with the neutron yield.

It has been shown that, at high excitation energies ($E_\gamma \gtrsim 100$ MeV), quasideuteron photodisintegration accompanied by the emission of more than one preequilibrium particle prevails.

ACKNOWLEDGMENTS

This work was supported in part by a grant (no. NSh-5365.2006.2) from the President of the Russian Federation for support of leading scientific schools.

REFERENCES

1. J. S. Levinger, Phys. Rev. **84**, 43 (1951).
2. J. R. Wu and C. C. Chang, Phys. Rev. C **16**, 1812 (1977).
3. M. Blann et al., Phys. Rev. C **28**, 2286 (1983).
4. M. B. Chadwick and P. G. Young, Acta Phys. Slovaca **45**, 633 (1995).
5. B. S. Ishkhanov and V. N. Orlin, Yad. Fiz. **66**, 1269 (2003) [Phys. At. Nucl. **66**, 1229 (2003)].
6. B. S. Ishkhanov and V. N. Orlin, Yad. Fiz. **67**, 614 (2004) [Phys. At. Nucl. **67**, 595 (2004)].
7. B. S. Ishkhanov and V. N. Orlin, Fiz. Élem. Chastits At. Yadra **38**, 460 (2007) [Phys. Part. Nucl. **38**, 232 (2007)].
8. J. S. Levinger, Phys. Lett. B **82**, 181 (1979).
9. M. B. Chadwick et al., Phys. Rev. C **44**, 814 (1991).
10. C. K. Cline and M. Blann, Nucl. Phys. A **172**, 225 (1971).
11. C. K. Cline, Nucl. Phys. A **210**, 590 (1973).
12. E. Gadioli, E. Gadioli Erba, and P. G. Sona, Nucl. Phys. A **217**, 589 (1973).
13. J. Dobes and E. Beták, Nucl. Phys. A **272**, 353 (1976).

14. M. Blann, Phys. Rev. Lett. **27**, 337 (1971).
15. M. Blann, Phys. Rev. Lett. **28**, 757 (1972).
16. M. Blann and H. K. Vonach, Phys. Rev. C **28**, 1475 (1983).
17. H. Feshbach, A. Kerman, and S. Koonin, Ann. Phys. (N. Y.) **125**, 429 (1980).
18. T. Tamura, T. Udagawa, and H. Lenske, Phys. Rev. C **26**, 379 (1982).
19. H. Nishioka et al., Ann. Phys. (N. Y.) **172**, 67 (1986).
20. H. Nishioka, H. A. Weidenmüller, and S. Yoshida, Ann. Phys. (N. Y.) **183**, 166 (1988).
21. J. M. Akkermans and A. J. Koning, Phys. Lett. B **234**, 417 (1990).
22. A. J. Koning and J. M. Akkermans, Ann. Phys. (N. Y.) **208**, 216 (1991).
23. A. J. Koning and M. B. Chadwick, Phys. Rev. C **56**, 970 (1997).
24. C. Kalbach, J. Phys. G **21**, 1519 (1995).
25. A. J. Koning and M. C. Duijvestijn, Nucl. Phys. A **744**, 15 (2004).
26. J. Bisplinghoff, Phys. Rev. C **33**, 1569 (1986).
27. M. Blann, Phys. Rev. C **54**, 1341 (1996).
28. M. Blann and M. B. Chadwick, Phys. Rev. C **57**, 233 (1998).
29. B. S. Ishkhanov and V. N. Orlin, Yad. Fiz. **71**, 517 (2008) [Phys. At. Nucl. **71**, 493 (2008)].
30. N. Bohr, Nature **137**, 344 (1936).
31. B. S. Ishkhanov and V. N. Orlin, Yad. Fiz. **66**, 688 (2003) [Phys. At. Nucl. **66**, 659 (2003)].
32. N. Stone, *Table of New Nuclear Moments*, Preprint 1997 (a revision of the *Table of Nuclear Moments*, by P. Raghavan, At. Data Nucl. Data Tables **42**, 189 (1989)) [http://www.nndc.bnl.gov/nndc/stone-moments].
33. V. S. Barashenkov and V. D Toneev, *Interactions of High-Energy Particles and Nuclei with Nuclei* (Atomizdat, Moscow, 1972) [in Russian].
34. S. C. Fultz et al., Phys. Rev. C **4**, 149 (1971).
35. B. S. Ishkhanov et al., Nucl. Phys. A **313**, 317 (1979).
36. S. C. Fultz et al., Phys. Rev. C **10**, 608 (1974).
37. J. Norbury et al., Austral. J. Phys. **31**, 471 (1978).
38. A. Lepretre et al., Nucl. Phys. A **367**, 237 (1981).
39. S. Fallieros and B. Goulard, Nucl. Phys. A **147**, 593 (1970).
40. R. Ö. Akyüz and S. Fallieros, Phys. Rev. Lett. **27**, 1016 (1971).
41. Nuclear Reaction Base Data, http://cdfe.sinp.msu.ru.

Translated by A. Isaakyan